On the Molecular and Electronic Structure of Spiroketones and Half-Molecule Models

V. Galasso*

Dipartimento di Scienze Chimiche, Università di Trieste, I-34127 Trieste, Italy

J. Bogdanov and P. Maslak

Department of Chemistry, The Pennsylvania State University, University Park, Pennsylvania 16802

D. Jones

Istituto dei Composti del Carbonio contenenti Eteroatomi e loro Applicazioni, C.N.R., via Gobetti 101, I-40129 Bologna, Italy

A. Modelli

Dipartimento di Chimica "G. Ciamician", Università di Bologna, via Selmi 2, I-40126 Bologna, Italy

Received: May 13, 2002; In Final Form: September 10, 2002

The equilibrium structures of three polyketones based on the 2,2′-spirobiindan skeleton (1,1′-dione, 1,3,1′-trione, and 1,3,1′,3′-tetraone), their "half-molecule" fragments (1-indanone and 2,2-dimethylindan-1,3-dione), and the indandione dimer (2,2′-dimethyl-[2,2′]-biindenyl-1,3,1′,3′-tetraone) were investigated using the density functional theory model B3LYP/6-31G(d,p). The results matched the X-ray experimental data that are available for one of the spiroketones. The electronic structure of these ketones was investigated by means of their spectroscopic properties. The NMR ^{13}C chemical shifts, calculated by the continuous-set-of-gauge-transformations formalism with the B3LYP/6-311+G(2d,p) method, were fairly consistent with NMR observations, in particular for the carbonyl, spiro, and quaternary carbons. The He(I) photoelectron spectra were measured and interpreted by means of ab initio outer-valence-Green's-function calculations. The theoretical results consistently reproduced the energies and splittings of the uppermost bands. These bands were associated with the phenyl π orbitals and the n(CO) lone-pair orbitals of the keto groups. Electron transmission spectroscopy, with the support of calculated π* virtual orbital energies, was employed to characterize the empty levels. Strong mixing between the phenyl and carbonyl π* fragment orbitals gave rise to stable anion states. Temporary anion states with mainly carbonyl character were observed in the 1.5−2.5 eV energy range. In the spiroketones, their energy splittings increase with the number of carbonyl groups present in the molecules and indicate the occurrence of through-space interactions between the two perpendicular indan halves.

Introduction

Nanotechnology requires the design of molecular devices with predictable electrooptical properties. In this field, spiroketones are compounds of current interest as potential three-dimensional acceptors.[1] Recently, in one of our laboratories, we have prepared several ketones,[2,3] based on the 2,2′-spirobiindan skeleton, which have been shown to be promising candidates for molecular charge-transfer relays by exploiting the phenomenon of spiroconjugation, i.e., the interaction between two perpendicular π planes.[4] Of these systems, the unsubstituted dione (**3**), trione (**4**), and tetraone (**5**) have been synthesized and characterized.[3] The parent monomeric fragments, 1-indanone (**1**) and 2,2′-dimethylindan-1,3-dione (**2**), as well as the indandione dimer (**6**) have long been documented in the literature[5−7] and serve here as "half-molecule" models for the spiroketones.

Given the systematically varied stereochemical disposition of the carbonyl groups, these compounds provide an opportunity for a combined experimental and theoretical investigation into the molecular and electronic structure of conjugated and spiroconjugated aromatic ketones. In the present paper, we report on calculations of the molecular and electronic structure of these compounds using density functional theory (DFT) and ab initio methodologies, and on the experimental probing of the electronic structure through the analysis of their ^{13}C NMR, photoelectron, and electron transmission spectra. The relevant spectroscopic properties are indeed very efficient monitors of the unique electronic interactions of the carbonyl groups in these molecules. In particular, the $\delta(^{13}C)$ spectroscopic parameters were studied using the continuous-set-of-gauge-transformations (CSGT) method, implemented with the B3LYP exchange-correlation DFT-HF hybrid functional. Photoelectron spectroscopy (PES) and electron transmission spectroscopy (ETS) were employed to determine the filled and empty electronic structures, respectively, of ketones **1**−**6** and to gain insight into the orbital interaction mechanisms. The vertical ionization energies (E_i's) measured in the He(I) PE spectra were interpreted by means of ab initio many-body calculations using the outer-valence-Green's-function (OVGF) method. The complementary ET spectra provided the vertical electron attachment energies (VAEs) into the empty molecular orbitals (MOs), i.e., the

* To whom correspondence should be addressed. E-mail: galasso@univ.trieste.it.

10.1021/jp021192i CCC: $22.00
Published on Web 10/15/2002

negative values of the electron affinities (E_{ea}'s) in the gas phase. This technique was employed to detect the formation of temporary anion states in the 0−6 eV energy range.

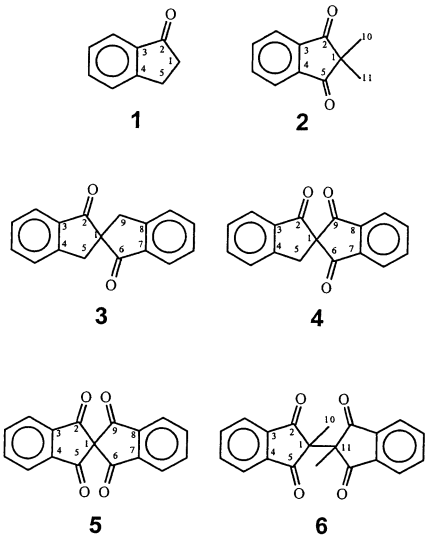

Experimental Details

1 was obtained from a commercial source. All other compounds were synthesized as previously described.[3] The He(I) spectra were recorded on a Perkin-Elmer PS-18 photoelectron spectrometer connected to a Datalab DL4000 signal analysis system. The bands, calibrated against rare-gas lines, were located using the position of their maxima, which were taken as corresponding to the vertical E_i values (±0.05 eV). The VAEs were measured by means of ETS. Our experimental setup is in the format devised by Sanche and Schulz[8] and has been previously described.[9] To enhance the visibility of the sharp resonance structures, the impact energy of the electron beam is modulated with a small ac voltage, and the derivative of the electron current transmitted through the gaseous sample is measured directly by a synchronous lock-in amplifier. The spectra were obtained in the "high-rejection" mode[10] and are therefore related to the nearly total scattering cross section. The electron beam resolution was about 50 meV (fwhm). The energy scale was calibrated with reference to the $(1s^22s^1)^2S$ anion state of He. The estimated accuracy of the measured VAEs is ±0.05 or ±0.1 eV, depending on the number of decimal digits reported. Furthermore, the collision chamber of the ETS apparatus has been modified[11] in order to allow for ion extraction at 90° with respect to the electron beam direction. Ions are then accelerated and focused toward the entrance of a quadrupolar mass filter. Alternatively, the total anion current can be collected and measured at the walls of the collision chamber (about 0.8 cm from the electron beam).

Computational Details

The equilibrium structures were completely optimized with the DFT/B3LYP hybrid functional[12] and the 6-31G(d,p) basis set by means of the Gaussian 98 suite of programs.[13] The combination of this functional, which takes into account the electron-correlation effects, and the polarized basis set offers a good compromise between the size of the calculations and the accuracy of the theoretical results. The ^{13}C NMR absolute shielding constants (σ values) were calculated at the B3LYP-DFT level with the CSGT method,[14] using the 6-311+G(2d,p) basis set. The calculated shieldings were converted to the δ chemical shifts by noting that at the same level of theory the ^{13}C absolute shielding in TMS is 177.54. The vertical E_is were calculated at the ab initio level according to Cederbaum's OVGF method,[15] which includes the effects of electron correlation and reorganization beyond the Hartree−Fock approximation, using the cc-pVDZ basis set[16] for all molecules. The self-energy part was expanded up to third order, and the contributions of higher orders were estimated by means of a renormalization procedure. To calculate the self-energy part, all occupied valence MOs and the 53, 66, 92, 92, 90, and 110 lowest virtual MOs were considered for **1**−**6**, respectively.

TABLE 1: Theoretical Structural Parameters (Bond Lengths in Å, Angles in Degrees)

	1	**2**	**3**	**4**	**5**	**6**
symmetry	C_s	C_{2v}	C_2	C_s	D_{2d}	C_{2h}
$r(C_1C_2)$	1.539	1.542	1.558	1.575	1.549	1.554
$r(C_1C_5)$	1.547		1.549	1.539		
$r(C_1C_6)$				1.542		
$r(C_1C_{10})$		1.540				1.538
$r(C_1C_{11})$						1.590
$\alpha(C_2C_1C_5)$	106.3	103.4	104.5	105.4	103.9	102.1
$\alpha(C_6C_1C_9)$				103.1		
$\alpha(C_{10}C_1C_{11})$		110.8				113.1
$\beta(C_2C_1C_6)$			106.3	107.8	112.3	
$\beta(C_2C_1C_9)$			110.9			
$\beta(C_5C_1C_9)$			119.1	116.2		
$\beta(C_2C_1C_{10})$		110.6				110.0
$\beta(C_2C_1C_{11})$						110.5

Results and Discussion

Molecular Structures. A selection of the most relevant geometrical parameters, related to the quaternary or spiro carbons, are collected in Table 1. As expected, there is a substantial resemblance in the structural patterns of the three spiroketones **3**−**5**, whose parameters are fairly well correlated with those of the corresponding half-molecule models **1** and **2**. Bond lengths and angles of **2** are in good accord with the relevant experimental data of the parent unsubstituted 1,3-indandione.[17] Also for tetraone **5**, the calculated structural parameters are in satisfactory agreement with the experimental X-ray data obtained by Maslak et al..[18] In particular, the pattern of $r(C_1C_2)$, $\alpha(C_2C_1C_5)$, and $\beta(C_2C_1C_6)$ in the spiro backbone of **5** is the following: 1.549 Å, 103.9°, and 112.3° (theoretical) versus 1.542 Å, 103.8°, and 112.4° (experimental). Lack of experimental data, however, precludes a similar comparison for the other molecules. All three spiroketones display a rigid structure, where the two planar indan halves are fused orthogonally. This arrangement allows for an efficient interaction between the two perpendicular π planes, as manifested by the UV absorption of the neutral spiroketones and by the ESR spectra of their radical anions.[2,3]

The most distinctive structural feature of the dimer **6**, which has a staggered conformation of C_{2h} symmetry, is the long central C−C bond of 1.590 Å. This bond is somewhat longer than that found in the isostructural molecule 2,2′-bis[2-(p-dimethylaminophenyl)indan-1,3-dione] (1.569 Å)[19] but similar to that determined in the related molecule 2,2′,3,3′-tetrahydro-2,2′dimethyl-[1,1′-bi-1H-indene]-1,1,2,2′-tetraol (1.605 Å).[20] As a consequence of this bond elongation, the intraring angle $\alpha(C_2C_1C_5)$ of the indandione moiety becomes more acute in the bridged molecule **6** (102.1°) than in the parent spiro molecule **5** (103.9°). Both through-bond interaction effects and steric repulsion are most likely responsible for the long C−C bond in **6**.

As a consequence of their peculiar stereochemistry, the patterns of the spectroscopic properties of these molecules

TABLE 2: ^{13}C NMR Chemical Shifts Relative to TMS

	theor	expt[a]	theor	expt[b]	theor	expt[b]
	1		**2**		**3**	
C_1	33.8	36.2	49.2	49.8	67.3	65.2
C_2	206.2	206.9	209.3	204.5	203.0	202.6
C_3	137.7	137.1	140.3	140.4	136.3	135.3
C_4	157.9	155.1			157.5	153.7
C_5	24.2	25.8			36.6	37.9
C_{10}			17.3	20.3		
	4		**5**		**6**	
C_1	74.2	73.0[b,c]	77.7	78.5	54.2	55.4
C_2	198.5	195.8	197.3	191.4	202.4	201.2
C_3	135.3	135.9	146.0	144.6	142.6	140.5
C_4	158.5	154.2				
C_5	29.9	31.9				
C_6	199.6	196.7				
C_7	145.0	143.8				
C_{10}					13.5	15.7

[a] Reference 21. [b] Reference 3. [c] The chemical shift of C_4 was incorrectly reported in ref 3.

exhibit important similarities and differences. Among the various spectroscopic observables, ^{13}C NMR chemical shifts, E_i's, and VAEs are very efficient monitors of the complex interplay of structural and electronic effects operating in a molecule. Therefore, we report here on these properties.

^{13}C Chemical Shifts. The most symptomatic ^{13}C chemical shifts of the investigated molecules are those of carbonyl carbon atoms. The results of the DFT-CSGT calculations together with the experimental values[3,21] are reported in Table 2. For all molecules, the overall agreement between theory and experiment is satisfactory. A comprehensive reproduction of the absolute values and main trends in the ^{13}C NMR spectra is observed.

In particular, the high deshielding of the carbonyl carbon atom in **1** is accounted for fairly well. Compared with the relevant chemical shifts of acetophenone (experimental 197.2,[22] our theoretical value 197.7) and benzaldehyde (experimental 193.8,[23] our theoretical value 192.0), the δ(CO) value of **1** is considerably upfield, likely because of steric differences with their consequent differences in intramolecular electronic interactions. The chemical shifts of carbonyl resonances along the series of ketones steadily decrease with increasing formal "ketonization". Additional carbonyl groups lower the chemical shift of the existing carbonyls, both through resonance effects (**1** versus **2** or **2** versus **4**) and inductive, through-bond, effects (**1** versus **3** or **3** versus **4**). The effect is sizable (experimental range $\Delta\delta = 11.2$) but exhibits some "saturation" (**3** versus **4**). On the other hand, the large difference ($\Delta\delta = 14.1$) between the tetracyclic dione **3** ($\delta = 202.6$) and the related bicyclic system (*R*)-spiro[4.4]-nonane-1,6-dione ($\delta = 216.7$)[24] may be viewed as a result of the transannular π,π interaction operative in **3**.

Similarly, a systematic progression is observed for C_1 resonances. Upon increasing substitution with carbonyl groups, the chemical shift of C_1 changes by nearly 30 ppm from $\delta = 49.8$ in **2** to $\delta = 78.0$ in **5**, an effect that is attributable to the inductive (through-bond) deshielding action of the C═O functionality. On the other hand, the close resemblance of the $\delta(C_1)$ values of **3** and the related bicyclic system (*R*)-spiro[4.4]-nonane-1,6-dione ($\delta = 64.4$)[24] indicates that only a modest deshielding is generated by the two fused benzene rings. All of these NMR spectroscopic features are accounted for fairly well by the present theoretical results.

Ionization Energies. The following aspects of the electronic structure of the molecules **1**−**6** are of special interest: (i) the splitting and evolution of the n E_i's associated with the carbonyl lone-pair orbitals (LPOs); (ii) the variation of the carbonyl π E_i's; and (iii) the behavior of the uppermost phenyl π E_i's. This information can be extracted from the PE spectra (Figures 1 and 2). The experimental E_i's together with the nonempirical OVGF results are reported in Table 3. For the sake of simplicity, some assignments are described with reference to the predominant character of the MO involved, in particular n, and π_{CO}, π_S, and π_A (the symmetric and antisymmetric, respectively, components of the parental benzene e_{1g} HOMO). Furthermore, $n^{\pm}$ and $\pi_{CO}^{\pm}$ represent the in-phase and out-of-phase, respectively, combinations of the relevant orbitals within one indan moiety. The labels $(\chi)^{\pm}$ indicate the bonding and antibonding combinations of the relevant χ orbitals of the two halves of the spiro molecule, respectively.

The results obtained by means of the same theoretical approach for some small, related molecules such as benzene, benzaldehyde, and indan were used as a yardstick for the assignments of **1**−**6**. The assignments advanced by Gleiter and Uschmann[25] for a series of heterospirenes were also taken into account. Thus, the first E_i of benzene is observed[26] at 9.25 eV and predicted by theory at 8.98 (π) eV. For benzaldehyde, the theory predicts 9.28 (π), 9.38 (π), 9.84 (n), 12.16 (σ), 12.37 (π_{CO}), and 12.61 (σ) eV, and the experiment[27] yields E_i's of 9.4 (π), 9.57 (n), 9.75 (π), 12.17 (σ), 12.47 (π_{CO}), and 12.82 (σ) eV. For indan, the theory predicts 8.15 (π) and 8.49 (π) eV and the experimental values are 8.46 and 9.04 eV.[28] Therefore, the theoretical formalism employed here suffers from an underestimation of the top phenyl $\pi_{S,A}$ E_i's, whereas it reproduces the n and π_{CO} E_i's more satisfactorily. To settle the specific assignments of **1**−**6**, the theoretical E_i's associated with the uppermost phenyl $\pi_{S,A}$ MOs were, therefore, raised by an average shift of 0.27 eV (i.e., the difference quoted for benzene). The assignments proposed in Table 3 are thus believed to provide a reasonably accurate interpretation of the photoionization processes of compounds **1**−**6**.

In the PE spectrum of **1**, the first complex band exhibits a peak at 9.05 eV and two discernible shoulders on the higher energy side. After a gap of 1 eV, there is the onset of a second prominent band. The theoretical results reported in Table 3 allow for a consistent assignment of this spectrum. In particular, the peak at 9.05 eV is generated by photoionization from the n LPO, whereas the two shoulders derive from the highest phenyl $\pi_{S,A}$ MOs. Both the absolute values of these E_i's and the splitting Δ between the two π E_i's are reproduced fairly well. The band observed between 11 and 12 eV in the spectra of **1** and **3** comprises photoionization both from the π_{CO} MO and from the outermost benzene σ MO. The cumulative inductive effect of the two carbonyl groups shifts the σ signal to higher energy in the dicarbonyl indan moiety with a consequent decrease in intensity of the 11−12 eV region of the spectra of indandione **2** and dimer **6**. The higher average π_{CO} E_i in spiro-tetraone **5** leads to the complete absence of bands in this energy range.

From a qualitative standpoint, on passing from **1** to **2**, the most noticeable difference is the presence of two n and π_{CO} semilocalized MOs. According to the assignment proposed for **2** in Table 3, the first band at 9.1 eV is attributed to the n^- MO. Photoionizations from the π_A and n^+ MOs give rise to the second band which peaks at 9.7 eV. Its shoulder at 10.1 eV should, therefore, be associated with the other benzene-like component, π_S. The $\pi_{CO}^{\pm}$ E_i's are correlated with higher energy bands. The theoretical average values and splittings Δ of the three distinct pairs n, π (benzene-like), and π_{CO} are in good agreement with the spectroscopic data. Furthermore, it is worthwhile mentioning that in the related monocyclic compound, 2,2-dimethyl-1,3-cyclopentanedione, the n^- and n^+ E_i

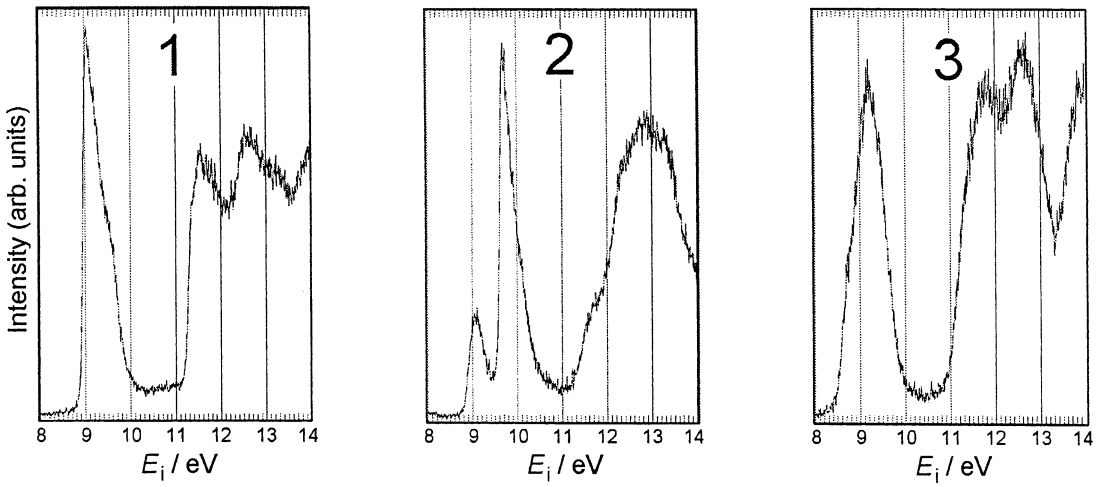

Figure 1. Ultraviolet He(I) photoelectron spectra of **1**−**3**.

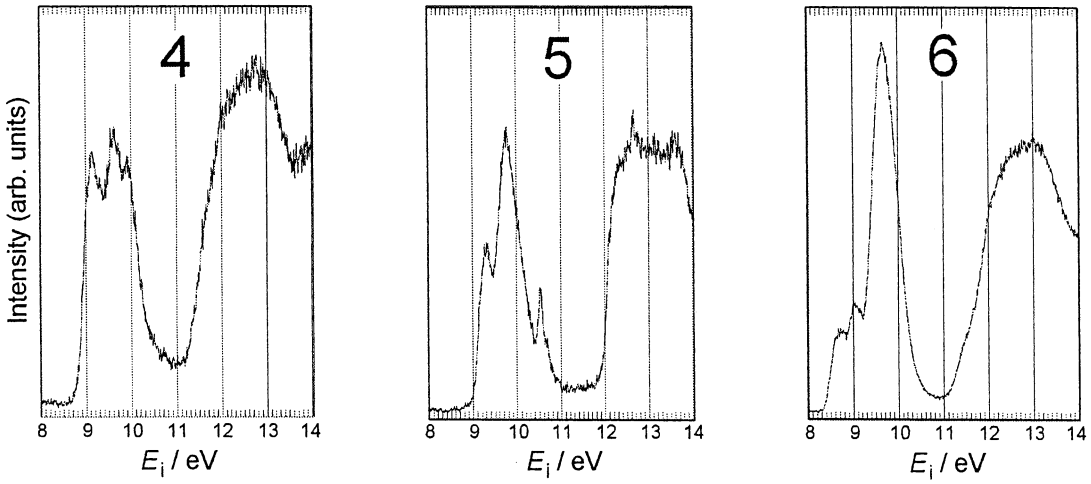

Figure 2. Ultraviolet He(I) photoelectron spectra of **4**−**6**.

values are 9.34 and 10.05 eV,[29] respectively. Compared with this molecule, the corresponding MOs in **2** undergo a nearly equal destabilization and Δ remains virtually unchanged. However, Δ(n) of **2** (0.6 eV) is slightly smaller than the average value of 0.8 eV determined for a number of simple β-dicarbonyls.[30]

Formal dimerization of **2** to give **6** is accompanied by doubling of the pairs n, π_{CO}, and $\pi_{S,A}$, which now interact through-space and through-bonds. Unfortunately, the congested low-energy bands of **6** do not allow for a detailed assignment of the various E_i's. However, by reference to the theoretical results in Table 3, it can be inferred that the overall splitting of the quartet of n E_i's of **6** ($\geq$1.0 eV) is considerably larger than Δ(n) of **2** (0.6 eV), indicating a considerable degree of interaction between the four LPOs of the composite molecule. The average n MO is only slightly destabilized, changing from 9.4 eV in **2** to 9.3 eV in **6**. In contrast, the whole manifold of the uppermost $\pi_{S,A}$ E_i's of **6** can be reasonably associated with the strong band centered at 9.7 eV. This energetic degeneracy, therefore, suggests that the intervening central σ(C−C) bond of **6** serves to *insulate* the two distant phenyl rings from each other.

Upon formal spiro connection of two monoketones **1** to give the spiro-dione **3**, both the average n and $\pi_{S,A}$ MOs undergo a slight destabilization. In particular, Δ(n) of the spiro β-dicarbonyl **3** (0.45 eV) is smaller than Δ(n) of the planar β-dicarbonyl **2** (0.6 eV), indicating that the planar conjugation of the two carbonyls in **2** (i.e., full delocalization of π electrons) is more effective than their spiro conjugation in **3**. Again, upon formal spiro connection of the two carbonyls **1** and **2** to give the spiro-trione **4**, both the average n (9.30 eV) and overall Δ(n) (0.75 eV) differ only slightly from those of the half-molecule **2**. This behavior may reflect a virtual balance of competing stereoelectronic interactions between the constituent moieties of **4**. On the other hand, formal spiro dimerization of **2** to give **5** generates a different pattern than that observed for the spiro dimerization **1** → **3**. Indeed, the average n MO becomes more tightly bound on passing from the precursor half-molecule **2** (9.4 eV) to spiro-tetraone **5** (9.74 eV). Furthermore, the overall Δ(n) doubles from 0.6 eV in **2** to 1.25 eV in **5**. Consequently, it can be concluded that a large degree of interaction occurs between the two spiro-linked orthogonal β-dicarbonyl skeletons of **5**.

The average values and splittings of the n E_i's along the examined set of spiroketones exhibit a rather monotonic pattern (8.98 and 0.45 eV (**3**), 9.30 and 0.75 eV (**4**), and 9.74 and 1.25 eV (**5**)), thereby indicating that the electronic influence exerted by progressive carbonylation of the 2,2′-spirobiindan skeleton is nearly additive. This outcome is consistent with the parallel upfield displacement observed for the corresponding carbonyl signals in the ^{13}C NMR spectra. Finally, it is worth mentioning that the π_{CO} E_i's follow a behavior similar to that of the related n E_i's, i.e., their average values and splittings increase in the sequence **3** < **4** < **5**. A comparison of the theoretical average π_{CO} E_i of spiro-tetraone **5** (12.9 eV) with that of the related

TABLE 3: Vertical Ionization Energies (E_i's in eV) and Assignment[a]

	assignment	$E_{i,theor}$	$E_{i,expt}$		assignment	$E_{i,theor}$	$E_{i,expt}$
1	n(a′)	9.13	9.05	**2**	$n^-(b_2)$	8.94	9.1
	π_S(a″)	9.22	9.25 sh		$\pi_A(b_1)$	9.55	9.7
	π_A(a″)	9.42	9.55 sh		$n^+(a_1)$	9.64	
	π_{CO}(a″)	11.70	11.55		$\pi_S(a_2)$	9.80	10.1 sh
	σ(a′)	11.74	11.8		$\pi_{CO}{}^+(b_1)$	11.60	11.6
	σ(a′)	12.21			$\sigma(a_1)$	12.19	
	π(a″)	12.71	12.6		$\pi(b_1)$	12.43	12.3
	σ(a′)	12.81			$\pi_{CO}{}^-(a_2)$	12.89	12.8
	π(a″)	13.53	13.2		$\sigma(a_1)$	13.01	
	σ(a′)	13.58			$\sigma(b_2)$	13.08	
	σ(a′)	14.20			$\sigma(b_2)$	13.18	
	σ(a′)	14.63			$\pi(b_1)$	13.25	
3	$(n)^-$(b)	8.84	8.75 sh	**4**	π_S(a″)	9.05	
	$(\pi_S)^-$(a)	8.97			n^-(a″)	9.08	9.15
	$(\pi_S)^+$(b)	9.15			n(a′)	9.10	
	$(\pi_A)^-$(a)	9.20	9.2		π_A(a″)	9.23	
	$(n)^+$(a)	9.23			π_A(a′)	9.41	9.6
	$(\pi_A)^+$(b)	9.24			π_S(a")	9.50	
	σ(b)	11.51	11.4 sh		n^+(a′)	10.03	9.9
	$(\pi_{CO})^-$(a)	11.68			$\pi_{CO}{}^+$(a′)	11.77	11.7 sh
	σ(b)	11.80	11.8		π_{CO}(a″)	11.95	
	σ(b)	11.83			σ(a′)	12.09	12.0 sh
	σ(a)	11.87			σ(a′)	12.10	
	σ(a)	12.46	12.6		σ(a′)	12.47	
	$(\pi_{CO})^+$(b)	12.61			$\pi_{CO}{}^-$(a″)	12.77	12.7
5	$(n^-)^{\pm}$(e)	9.20	9.3	**6**	$(n^-)^+(b_g)$	8.42	8.7
	$(n^+)^-(b_2)$	9.50	9.8		$(n^+)^+(a_g)$	9.23	9.0
	$\pi_A{}^{\pm}$(e)	9.64			$\pi_A(b_u)$	9.31	
	$\pi_S{}^-(a_2)$	9.89	10.1 sh		$\pi_A(a_g)$	9.37	
	$\pi_S{}^+(b_1)$	9.89			$\pi_S(b_g)$	9.44	
	$(n^+)^+(a_1)$	10.66	10.55		$(n^-)^-(a_u)$	9.46	9.7
	$(\pi_{CO}{}^+)^{\pm}$(e)	12.33	12.3		$\pi_S(a_u)$	9.47	
	$\sigma(b_2)$	12.52			$(n^+)^-(b_u)$	9.96	
	$\sigma(a_1)$	12.68	12.7		$\pi_{CO}(a_g)$	11.13	11.4 sh
	$(\pi_{CO})^-(a_2)$	12.99			$\pi_{CO}(b_u)$	12.00	
	σ(e)	13.15	13.2		$\sigma(a_g)$	12.01	
	σ(e)	13.65			$\sigma(a_g)$	12.23	12.3 sh
	$\sigma(b_2)$	13.90	13.7		$\sigma(b_u)$	12.31	
	$(\pi_{CO}{}^-)^+(b_1)$	13.94			$\pi_{CO}(b_g)$	12.56	

[a] The theoretical uppermost phenyl $\pi_{S,A}$ E_i's are raised by a factor of 0.27 eV, see text.

ethano-bridged tetraone **6** (12.2 eV) suggests a larger through-bond interaction transmitted across the spiro junction of two indandione moieties.

Electron Attachment Energies. Figure 3 shows the ET spectra of **1**−**6** in the 0−6 eV range. The measured VAEs are reported in the diagram of Figure 4 and in Table 4, where, by reference to their main character, the empty MOs are labeled as π^*_S, π^*_A* (the symmetric and antisymmetric, respectively, components of the benzene e_{2u} LUMO), π^*_{CO}, and π^*_O (the total antibonding benzene b_{2g} MO mixed with the π^*_{CO} MO).

As expected, the spectrum of **1** displays three resonances close in energy to those of benzaldehyde and acetophenone.[31] The degeneracy of the parental benzene LUMO (VAE = 1.12 eV)[9] is removed by interaction with the carbonyl group (VAE = 1.31 eV for π^*_{CO} of acetone).[32] Owing to this strong mixing, the π^*_S LUMO gives rise to a stable anion state, not observable in ETS. The first resonance displayed by the ET spectrum (0.72 eV) is associated with the noninteracting benzene π^*_A MO, inductively stabilized, whereas the mainly π^*_{CO} MO yields the resonance at 2.40 eV. Furthermore, electron capture into the highest-lying π^*_O MO generates the feature at 4.4 eV. Its fwhm is 0.9 eV compared with 0.55 eV in acetophenone,[31] which suggests the presence of an unresolved contribution due to a core-excited resonance, i.e., electron capture accompanied by simultaneous excitation of the neutral molecule.

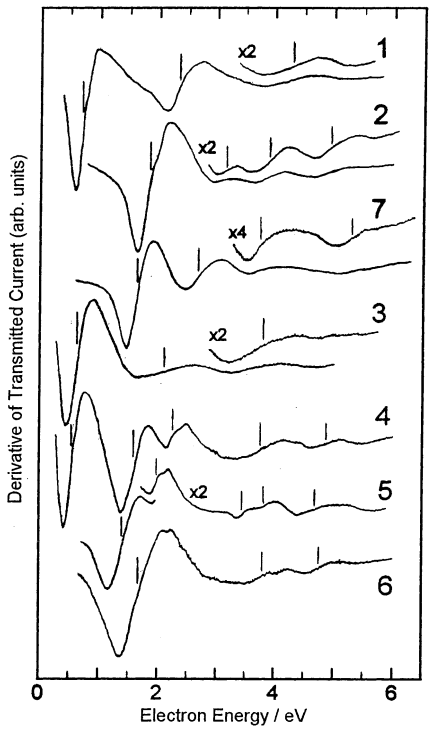

Figure 3. Electron transmission spectra of **1**−**6** and phthalic anhydride (**7**). Vertical lines locate the most probable VAEs.

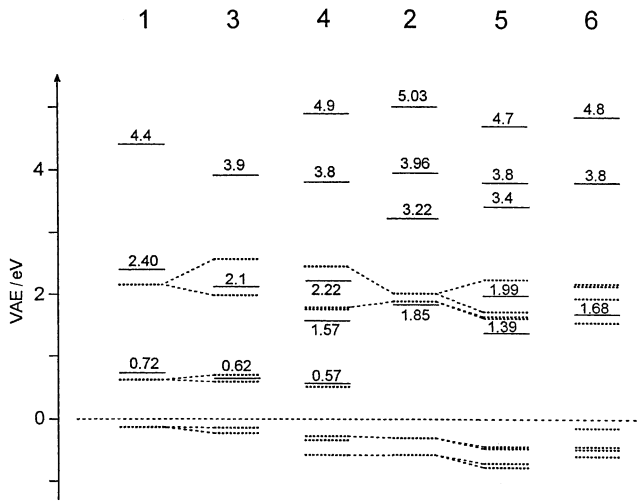

Figure 4. Correlation diagram of the π^* VAEs (dashed lines) of **1**−**6**, obtained from the calculated empty MO energies of the neutral molecules and the linear regression given in ref 34. The experimental VAEs (full lines) are also reported.

The ET spectrum of spiro-dione **3** closely resembles that of the parent half-molecule **1**. Indeed, the first two resonances, each associated with the unresolved contributions of the two perpendicular π^*_A and π^*_{CO} MOs, respectively, are slightly shifted to lower energy by a mutual electron-withdrawing effect of the two molecular halves. A significant difference from **1** is that the second resonance is 0.4 eV broader, thus indicating an energy splitting of 0.3−0.4 eV between the two π^*_{CO} anion states of **3**, consistent with the occurrence of through-space interaction.

In 2,2′-dimethylindan-1,3-dione (**2**), the presence of two carbonyl substituents reorients the two components of the benzene e_{2u} (π^*) MO, so that the π^*_A MO possesses the largest wave function coefficients at the substituted carbon atoms. Three

TABLE 4: Experimental Vertical Attachment Energies (VAEs) and fwhms, Calculated Orbital Energies ϵ_{π^*} (eV) and Assignment

	VAE (fwhm)	ϵ_{π^*}	assignment[a]
1	4.4 (0.9)		π^*_O + c.e.
	2.40 (0.60)	2.15	$\pi^*_{CO}(a'')$
	0.72 (0.39)	0.61	$\pi^*_A(a'')$
	<0	−0.12	$\pi^*_S(a'')$
2	5.03 (0.70)		c.e.
	3.96 (0.55)		π^*_O
	3.22 (0.31)		c.e.
	1.85 (0.56)	1.88, 2.02	$\pi^*_{CO}{}^+(b_1)$, $\pi^*_{CO}{}^-(a_2)$
	<0	−0.57, −0.27	$\pi^*_S(a_2)$, $\pi^*_A(b_1)$
3	3.9 (1.1)		$2\pi^*_O$ + c.e.
	2.1 (1.0)	1.98, 2.58	$2\pi^*_{CO}(a,b)$
	0.62 (0.43)	0.57, 0.68	$2\pi^*_A(a,b)$
	<0	−0.21, −0.16	$2\pi^*_S(a,b)$
4	4.9 (0.42)		c.e.
	3.8 (0.8)		$2\pi^*_O$
	2.22 (0.35)	2.47	$\pi^*_{CO}{}^-(a'')$
	1.57 (0.45)	1.76, 1.77	$\pi^*_{CO}(a'')\cdot\pi^*_{CO}{}^+(a')$
	0.57 (0.45)	0.55	$\pi^*_A(a'')$
	<0	−0.31	$\pi^*_S(a')$
	<0	−0.57, −0.34	$\pi^*_A(a'')\cdot\pi^*_S(a'')$
5	4.7 (0.8)		c.e.
	3.84 (0.3)		$2\pi^*_O$
	3.44 (0.3)		c.e.
	1.99 (0.32)	2.28	$(\pi^*_{CO}{}^-)^-(a_2)$
	1.39 (0.51)	1.64, 1.71	$(\pi^*_{CO}{}^+)^{\pm}$(e), $(\pi^*_{CO}{}^-)^+(b_1)$
	<0	−0.45	π^*_S(e)
	<0	−0.74, −0.69	$\pi^*_A{}^+(b_1)$, $\pi^*_A{}^-(a_2)$
6	4.8 (0.5)		c.e.
	3.8 (0.5)		$2\pi^*_O$
		2.12, 2.14	$(\pi^*_{CO}{}^-)^-(b_g)$, $(\pi^*_{CO}{}^+)^-(a_g)$
	1.68 (0.82)	1.54, 1.93	$(\pi^*_{CO}{}^+)^+(b_u)$, $(\pi^*_{CO}{}^-)^+(a_u)$
	<0	−0.45, −0.15	$\pi^*_S{}^+(b_u)$, $\pi^*_S{}^-(a_g)$
	<0	−0.58, −0.48	$\pi^*_A{}^+(a_u)$, $\pi^*_A{}^-(b_g)$

[a] c.e. stands for core-excitation.

empty MOs of a_2 symmetry derive from interaction of the $\pi^*_{CO^-}$ combination with the π^*_A and π^*_O ring orbitals and two MOs of b_1 symmetry are obtained by mixing the π^*_S ring MO with the $\pi^*_{CO^+}$ combination. The ET spectrum displays no resonance at low energy, thus indicating that the first two anion states (π_A^* and π_S^*) are stable. In the spectrum, the first resonance appears at 1.85 eV, followed by weaker signals at 3.22, 3.96, and 5.03 eV. The energy of the latter two signals is consistent with their assignment to the highest-lying π^*_O MO and a core-excited process, likely mixed together. The assignment of the resonances at 1.85 and 3.22 eV is not straightforward. The former could be due to the unresolved contributions of both the $\pi^*_{CO^+}$ and $\pi^*_{CO^-}$ MOs. In this case, the two anion states should be very close in energy because the resonance width (<0.6 eV) is relatively narrow, and the signal at 3.22 eV may thus arise from a core-excited resonance. Alternatively, the 1.85 and 3.22 eV resonances could be associated with $\pi^*_{CO^+}$ and $\pi^*_{CO^-}$ MOs, respectively.

To get some insight into the assignment of the ET spectrum of **2**, which is a basis for the interpretation of the spectrum of spiro-tetraone **5**, we used a simple LCBO approach,[33] applied to the interaction among the empty π^* orbitals of the phenyl and carbonylic groups. The Coulomb (A) and resonance (B) integrals were derived from the experimental VAEs of the reference molecules, p-benzoquinone, acetaldehyde, and acetophenone.[31] By accounting for the different overlap and wave function coefficients and by assuming that each carbonyl group inductively stabilizes the other group orbitals by 0.3 eV, the following parameters were obtained: $A(\pi_A^*) = A(\pi_S^*) = 0.5$ eV, $A(\pi^*_{CO^+}) = A(\pi^*_{CO^-}) = 1.0$ eV, $A(\pi_O^*) = 4.2$ eV, $B(\pi^*_{CO^-}/\pi_A^*) = -1.73$ eV, $B(\pi^*_{CO^-}/\pi_O^*) = -1.41$ eV, and $B(\pi^*_{CO^+}/\pi_S^*) = -1.00$ eV. The secular determinant leads to the π^* MO energies of −1.16 (a_2), −0.28 (b_1), 1.78 (b_1), 2.03 (a_2), and 4.83 (a_2) eV. These results confirm the stability of the first two anion states, and in particular, the VAEs (1.9 ± 0.1 eV) of the $\pi^*_{CO^+}$ and $\pi^*_{CO^-}$ anions are predicted to be very close each other and to the energy of the 1.85 eV resonance, supporting its assignment to both anions. An independent test for this assignment is supplied by the ET spectrum of phthalic anhydride (referred to as compound **7** in Figure 3), by taking advantage of the sizable destabilization (1.3 eV in cyclopent-2-en-1,3-dione)[32] of the $\pi^*_{CO^+}$ MO by mixing with an adjacent oxygen LPO. In agreement with the assignment of the resonance at 1.85 eV to both anion states in **2**, the spectrum of **7** shows the $\pi^*_{CO^-}$ resonance, slightly inductively stabilized, at 1.64 eV (fwhm = 0.43 eV) and the $\pi^*_{CO^+}$ resonance at 2.76 eV.

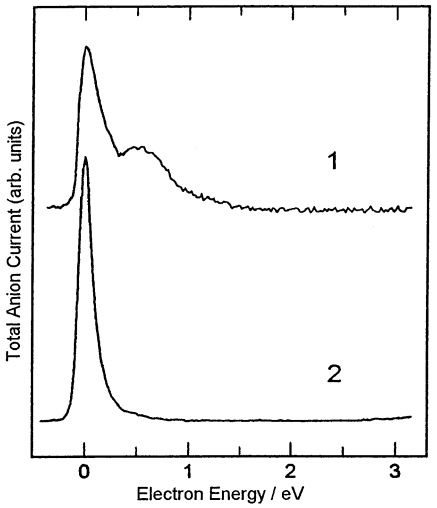

Figure 5. Total anion current measured in **1** and **2** at the walls of the collision chamber, as a function of the incident electron energy.

Measurements of the negative ion yield as a function of the incident electron energy (dissociative electron attachment spectroscopy or DEAS) in molecular systems, which possess stable anion states, often display a zero-energy peak associated with formation of long-lived vibrationally excited molecular anions and/or fragment anions generated by its dissociation. To obtain direct experimental evidence for the presence of stable anion states in **1** and **2**, we recorded the total anion current measured at the walls of the collision chamber, as shown in Figure 5. In both compounds, a zero-energy peak is observed, consistent with the presence of stable anion states. In **1**, a second low-energy maximum (0.5 eV) is also displayed, associated with the π^*_A resonance located at 0.72 eV in the ET spectrum. Moreover, anion extraction and mass analysis through a quadrupole mass filter (which requires a lifetime $\geq 10^{-6}$ s) revealed only one zero-energy peak in **2**, because of the molecular anion. Thus, also in **1**, the low-energy signals observed in the total anion current are probably due to the molecular anion, but with too short a lifetime to be detected through a mass filter.

In the ET spectrum of spiro-trione **4** the first resonance (0.57 eV) is clearly associated with the π^*_A MO of the indanone moiety. The corresponding π^*_S anion state and the two lowest anion states of the dione moiety are expected to be stable, as is the case in **1** and **2**. The next two resonances are located at 1.57 and 2.22 eV. The near degeneracy of the $\pi^*_{CO^+}$ and $\pi^*_{CO^-}$ MOs of **2** (Figure 4) should be removed because only the latter has the proper symmetry to mix with the perpendicular π^*_{CO}

MO. The 1.57 eV resonance is therefore assigned to the indanone π^*_{CO} and dione $\pi^*_{CO^+}$ MOs and the 2.22 eV resonance to the $\pi^*_{CO^-}$ MO.

In spiro-tetraone **5**, each of the π^* MOs of **2** has a perpendicular counterpart and mutual inductive stabilization of the two halves should occur. Symmetry considerations (D_{2d}) reveal that each of the two pairs of the perpendicular π^*_S and $\pi^*_{CO^+}$ MOs of **2** gives rise to a degenerate state. Thus, the first three π^* anion states (with b_1, a_2, and e symmetry) are expected to be stable and the next three anion states to fall in the energy range of the 1.85 eV resonance of **2**. Accordingly, the ET spectrum of **5** displays the first two resonances at 1.39 and 1.99 eV. Their relative intensities and widths suggest that the former is associated with the degenerate $\pi^*_{CO^+}$ MOs and the bonding combination of the $\pi^*_{CO^-}$ MOs, whereas the latter is associated with the antibonding combination of the $\pi^*_{CO^-}$ MOs. The splitting (0.6 eV) between the $(\pi^*_{CO^-})^{\pm}$ MOs and their barycenter (1.7 eV) indicates the occurrence of a significant through-space interaction between the carbonyl empty π^* MOs of the two perpendicular fragments. As a consequence, the corresponding bonding and antibonding combinations span the entire molecule, in agreement with the conclusion drawn from the ESR spectrum of the ground anion state.[2]

Finally, in the ET spectrum of the dimer **6**, a single unresolved resonance is observed in the energy range of the four empty π^* MOs with mainly carbonyl character, centered at 1.68 eV. This signal is rather broad but narrower than in spiro-dione **3**. This finding suggests that the degree of mixing of the two bridged parallel 1,3-dione π-systems is smaller than in the perpendicular spiro-analogue **5**.

It is well-known that the virtual MO energies supplied by HF Koopmans' theorem calculations are much higher than the experimental VAEs, because of the neglect of the correlation and relaxation effects. However, analysis of the calculated and experimental π^* MO energies in a large number of molecules demonstrated a good correlation between the two sets of data.[34] Therefore, we applied the linear regression found for the 6-31G* basis set, similar to that employed in the present OVGF calculations, to evaluate the lowest π^* VAEs of **1**−**6**. (As to the basis set employed here, it should be mentioned that, according to the analysis by Staley and Strnad,[34] the use of diffuse functions is not recommended for KT calculations of *unbound* π^* negative ion states.) These theoretical values, reported in Table 4 and in Figure 4, closely match the measured VAEs and support the assignments advanced above. In particular, the energy proximity of the $\pi^*_{CO^+}$ and $\pi^*_{CO^-}$ MOs in **2** and the splittings between the mainly carbonyl π^* MOs of the two perpendicular halves in spiro-compounds **3**−**5** are reasonably well reproduced. Furthermore, it can be noted that the corresponding splittings between the stable anion states, which possess the same symmetries, are predicted to be smaller, in line with their smaller localization at the carbonyl groups.

Concluding Remarks

The equilibrium structures of three spiroketones, based on the 2,2′-spirobiindan skeleton, their half-molecule models and a dimeric indandionic system have been studied with the density functional method B3LYP/6-31G(d,p). The electronic structure of these functionalized polycycles has been investigated with their ^{13}C NMR, PE, and ETS spectroscopic properties. On the whole, the correspondence between experimental data and theoretical values, obtained by high-level calculations, is satisfactory. In particular, the variations in the ^{13}C NMR chemical shifts of the spiro and carbonyl carbons were correctly accounted for by the CSGT predictions. A detailed assignment of the low-lying bands in the PE spectra has also been proposed. The OVGF results yielded a consistent description of the main features in the PE spectra, i.e., location, splitting, and sequence of the n, π_{CO}, and π-phenyl MOs. These data indicate a sizable interaction between the filled orbitals of the two perpendicular halves through the σ bonds of the spiro junction. The ETS technique was employed to locate the temporary anion states generated by electron attachment to the empty MOs. In all of the ketones considered, the LUMO gives rise to a stable anion state (positive electron affinity), owing to strong mixing between the π^* empty orbitals of the phenyl and carbonyl groups. The ET spectra of the spiroketones show significant energy splittings between the anion states with mainly carbonyl character. In line with the spatial diffuseness of the anion states, these data are consistent with through-space interaction between the carbonyl groups of the two perpendicular halves. Both PE and ET data gave evidence of an increased degree of electronic interaction between the two indan halves with progressive carbonylation at the positions adjacent to the central carbon atom.

Acknowledgment. Financial support from MIUR of Italy is gratefully acknowledged by V.G. and A.M., who also acknowledges the support from Funds for Selected Topics of the Dipartimento di Chimica "G. Ciamician" of the University of Bologna.

References and Notes

(1) Maslak, P. *Adv. Mater.* **1994**, *6*, 405.
(2) Maslak, P.; Augustine, M. P.; Burkey, J. D. *J. Am. Chem. Soc.* **1990**, *112*, 5359.
(3) Maslak, P.; Varadarajan, S.; Burkey, J. D. *J. Org. Chem.* **1999**, *64*, 8201.
(4) Durr, H.; Gleiter, R. *Angew. Chem., Int. Ed. Engl.* **1978**, *17*, 559.
(5) Wislicenus, W.; Kotzle, A. *Justus Liebig Ann. Chem.* **1889**, *86*, 252.
(6) Spencer, T. A.; Hall, A. L.; Fordham von Reyn, C. *J. Org. Chem.* **1968**, *33*, 3369.
(7) House, H. O.; McDaniel, W. C. *J. Org. Chem.* **1977**, *42*, 2155.
(8) Sanche, L.; Schulz, G. J. *J. Phys. Rev.* **1972**, *A5*, 1672.
(9) Modelli, A.; Jones, D.; Distefano, G. *Chem. Phys. Lett.* **1982**, *86*, 434.
(10) Johnston, A. R.; Burrow, P. D. *J. Electron Spectrosc. Relat. Phenom.* **1982**, *25*, 119.
(11) Modelli, A.; Foffani, A.; Scagnolari, F.; Jones, D. *Chem. Phys. Lett.* **1989**, *163*, 269.
(12) Becke, A. D. *J. Chem. Phys.* **1993**, *98*, 5648.
(13) Frisch, M. J.; Trucks, G. W.; Schlegel, H. B.; Scuseria, G. E.; Robb, M. A.; Cheeseman, J. R.; Zakrzewski, V. G.; Montgomery, J. A., Jr.; Stratmann, R. E.; Burant, J. C.; Dapprich, S.; Millam, J. M.; Daniels, A. D.; Kudin, K. N.; Strain, M. C.; Farkas, O.; Tomasi, J.; Barone, V.; Cossi, M.; Cammi, R.; Mennucci, B.; Pomelli, C.; Adamo, C.; Clifford, S.; Ochterski, J.; Petersson, G. A.; Ayala, P. Y.; Cui, Q.; Morokuma, K.; Malick, D. K.; Rabuck, A. D.; Raghavachari, K.; Foresman, J. B.; Cioslowski, J.; Ortiz, J. V.; Stefanov, B. B.; Liu, G.; Liashenko, A.; Piskorz, P.; Komaromi, I.; Gomperts, R.; Martin, R. L.; Fox, D. J.; Keith, T.; Al-Laham, M. A.; Peng, C. Y.; Nanayakkara, A.; Gonzalez, C.; Challacombe, M.; Gill, P. M. W.; Johnson, B. G.; Chen, W.; Wong, M. W.; Andres, J. L.; Head-Gordon, M.; Replogle, E. S.; Pople, J. A. *Gaussian 98*, revision A.6; Gaussian, Inc.: Pittsburgh, PA, 1998.
(14) Keith, T. A.; Bader, R. F. W. *Chem. Phys. Lett.* **1993**, *210*, 223.
(15) Cederbaum, L. S. *J. Phys. B* **1975**, *8*, 290.
(16) Woon, D. E.; Dunning, T. H., Jr. *J. Chem. Phys.* **1993**, *98*, 1358.
(17) Bravic, G.; Bechtel, F.; Gaultier, J.; Hauw, C. *Cryst. Struct. Comm.* **1976**, *5*, 1.
(18) Maslak, P.; Varadarajan, S.; Rheingold, A. L.; Yap, G. P. To be published.
(19) Aliev, Z. G.; Chekhlov, A. N.; Atovmyan, L. O.; Pisarenko, L. M.; Nikulin, V. I. *Zh. Strukt. Khim.* **1990**, *31*, 103.
(20) Delaunay, J.; Orliac-Le Moing, A.; Lebouc, A.; Simonet, J.; Toupet, L. *J. Chem. Res. (S)* **1986**, 418.
(21) Boykin, D. W.; Hertzler, R. L.; Delphon, J. K.; Eisenbraun, E. J. *J. Org. Chem.* **1989**, *54*, 1418.
(22) Beistel, D. W.; Edwards, W. *J. Phys. Chem.* **1976**, *80*, 2023.

(23) de Kowalewski, D. G.; Kowalewski, V. J.; Botek, E.; Contreras, R. H.; Facelli, J. C. *Magn. Reson. Chem.* **1997**, *35*, 351.
(24) Suemune, H.; Maeda, K.; Kato, K.; Sakai, K. *J. Chem. Soc., Perkin Trans. 1* **1994**, 3441.
(25) Gleiter, R.; Uschmann, J. *J. Org. Chem.* **1986**, *51*, 370.
(26) Kimura, K.; Katsumata, S.; Achiba, Y.; Yamazaki, T.; Iwata, S. *Handbook of HeI Photoelectron Spectra of Fundamental Organic Molecules*; Halsted: New York, 1981.
(27) Klasinc, L.; Kovač, B.; Güsten, H. *Pure Appl. Chem.* **1983**, *55*, 289. Klasinc, L.; Novak, I.; Sabljić, A.; McGlynn, S. P. *Int. J. Quantum Chem.: Quantum Biol. Symp.* **1988**, *15*, 259.
(28) Santiago, C.; Gandour, R. W.; Houk, K. N.; Nutakul, W.; Cravey, W. E.; Thummel, R. P. *J. Am. Chem. Soc.* **1978**, *100*, 3730.
(29) Houk, K. N.; Davis, L. P.; Newkome, G. R.; Duke, R. E., Jr.; Nauman, R. V. *J. Am. Chem. Soc.* **1973**, *95*, 8364.
(30) Dougherty, D.; Brint, P.; McGlynn, S. P. *J. Am. Chem. Soc.* **1978**, *100*, 5597.
(31) Modelli, A.; Burrow, P. D. *J. Phys. Chem.* **1984**, *88*, 3550.
(32) Modelli, A.; Distefano, G.; Jones, D. *Chem. Phys.* **1982**, *73*, 395.
(33) Heilbronner, E.; Bock, H. *The HMO Model and Its Applications*; Wiley: Chichester, U.K., 1976.
(34) Staley, S. W.; Strnad, J. T. *J. Phys. Chem.* **1994**, *98*, 116.